On Stratified Kolmogorov Flow

Yuan-nan Young

Abstract

In this study we investigate the stability of the weakly stratified Kolmogorov shear flow. We derive the amplitude equations for this system and solve them numerically to explore the effect of weak stabilizing stratification. We then explore the non-diffusive limit of this system and derive amplitude equations in this limit.

1 Introduction

The Kolmogorov flow - a two-dimensional viscous sinusoidal flow induced by a unidirectional external force field - has been studied in the context of generation of large scale turbulence in two-dimension. Various aspects of the Kolmogorov flow, such as the generation of 2D turbulence [1], vortex merging [2], and the negative viscosity in the role of large scale formation in 2D turbulence [3], have been widely applied to geophysical [4] and laboratory systems [5, 6].

In this study we impose a weak, stabilizing temperature gradient and investigate the temperature evolution associated with the flow instability. We first adopt Sivashinsky's approach and derive the finite-amplitude equation for the case of infinite domain (periodic boundary conditions) and finite Peclet numbers. We then solve the amplitude equations (both 1D and 2D) numerically and investigate the buoyancy effect on the structure formation of the flow. We also investigate large Peclet number cases, where the critical layers in the scalar field plays a key role for the flow instability and dynamics. We also make comparison between fully numerical simulations and results from the weakly nonlinear analyses.

2 Formulation and linear analysis

2.1 Formulation

The Kolmogorov shear flow is more generally defined as a sinusoidal shear flow, whether the fluid is viscous or inviscid. In our 2-D formulation of the problem, where the incompressible flow can be written as a stream function, we couple this background shear flow to a stabilizing temperature. Without loss of generality, we write the total background state as a sinusoidal stream function and a linear temperature profile:

$$\Psi_0 = U_0 l \cos(z/l), \quad T_0 = \frac{\triangle T}{l} z, \tag{1}$$

where U_0 is the amplitude of the background shear flow, l is the periodicity of the shear flow, and $\triangle T$ is the temperature difference across distance l. Denoting ψ as the stream function

disturbance and θ as the temperature disturbance, we first write the momentum equation and the advection diffusion equation as follows:

$$\partial_t \nabla^2 \psi + \partial_x(\partial_z \Psi_0 \nabla^2 \psi - \partial_z^3 \Psi_0 \psi) - J(\psi, \nabla^2 \psi) = \nu \nabla^4 \psi - g\alpha\theta_x, \tag{2}$$

$$\partial_t \theta + \partial_z \Psi_0 \partial_x \theta - \partial_x \psi \partial_z T_0 - J(\psi, \theta) = \kappa \nabla^2 \theta. \tag{3}$$

We nondimensionalize the above equations such that the background shear flow $u_0 = -\sin z$ and the background stabilizing thermal gradient is equal to 1 ($\mathrm{Re} \equiv U_0 l/\nu$ is the Reynolds number, $\mathrm{Pe} \equiv U_0 l/\kappa$ is the Peclet number, and $\mathrm{Ri} \equiv g\alpha\delta T l^2/U_0^2$ is the Richardson number), and equations 2 and 3 thus read:

$$\partial_t \nabla^2 \psi - \sin z(\nabla^2 \psi + \psi)_x - J(\psi, \nabla^2 \psi) = \frac{1}{\mathrm{Re}} \nabla^4 \psi - \mathrm{Ri}\theta_x, \tag{4}$$

$$\partial_t \theta - (\sin z \theta + \psi)_x - J(\psi, \theta) = \frac{1}{\mathrm{Pe}} \nabla^2 \theta. \tag{5}$$

In the following subsections we first present results from the usual linear analysis on cases where the periodicity of the shear flow is the same as the domain considered (integer periodicity). We then consider cases where the perturbations are products of periodic and exponential functions (Floquet system) and may exhibit parametric resonance.

2.2 Linear analysis on the stratified Kolmogorov flow

In this section we present results of linear analysis on equations 4 and 5 for shear flow of periodicity the same as the domain size. The linearized version of equations 4 and 5 read

$$\partial_t \nabla^2 \psi - \sin z \partial_x(\nabla^2 \psi + \psi) = \frac{1}{\mathrm{Re}} \nabla^4 \psi - \mathrm{Ri}\theta_x, \tag{6}$$

$$\partial_t \theta - (\sin z \theta + \psi)_x = \frac{1}{\mathrm{Pe}} \nabla^2 \theta. \tag{7}$$

Without the stabilizing temperature, the non-stratified Kolmogorov shear flow is known to be unstable to long wave length perturbation for Reynolds numbers $\mathrm{Re} > \sqrt{2}$: the critical wave number $k_c = 0$ and the critical Reynolds number $\mathrm{Re}_c = \sqrt{2}$. Also for small horizontal wave numbers ($k \ll 1$) the growth rate λ can be obtained via the following dispersion relation:

$$\lambda = (1 - \frac{\mathrm{Re}^2}{2})k^2 + \mathrm{Re}^2(1 + \frac{\mathrm{Re}^2}{4})k^4 + \mathcal{O}(k^6). \tag{8}$$

We numerically solve the above linearized equations with periodic boundary conditions (in both the horizontal and the vertical directions). Figure 1 shows marginal curves for weak stratification (see caption for the corresponding stratification strength for each curve) and figure 2 shows the critical Reynolds numbers and wave numbers as functions of Richardson numbers for Prandtl number $\mathrm{Pr} \equiv \nu/\kappa = 10$. As shown in the figures, the critical wave number k_c increases rapidly as we increase the Richardson number above. As the Richardson number increases above 10^{-5}, the critical wave number k_c increases significantly from 0 towards some finite value (~ 0.1). This also implies that the inverse cascade observed in the nonstratified Kolmogorov shear flow is at risk, namely, the large scale perturbation now has been stabilized by the existence of the stably stratified temperature. As will be shown in the numerical results, the inverse cascade is indeed prevented by the stabilizing temperature and we will discuss this in detail via the tool of Lyapunov functional.

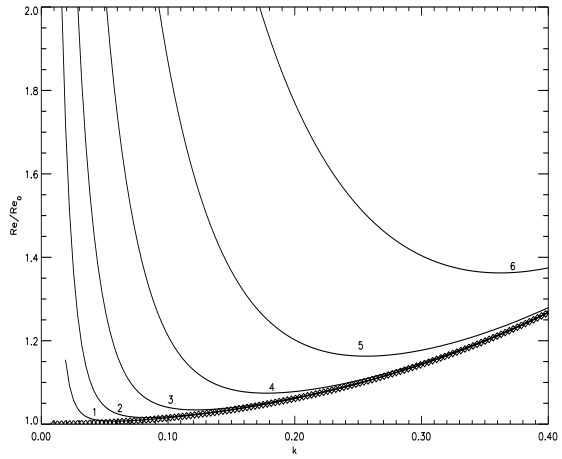

(a)

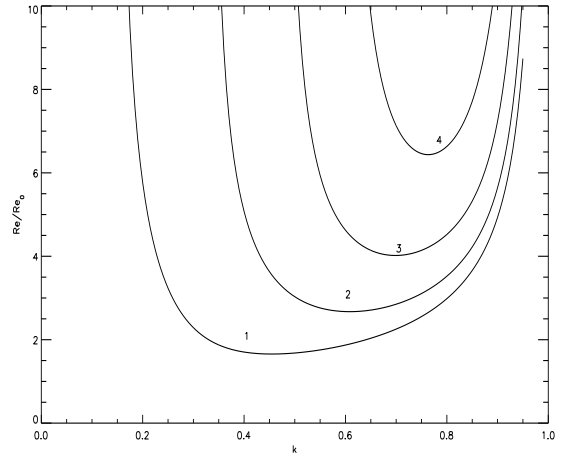

(b)

Figure 1: Marginal curves for the unbounded stratified Kolmogorov flow for weak stratification and Prandtl number $\sigma = 1$. Curves are labeled by their Richardson numbers. In Panel (a), from curve 1 to curve 6, the Richardson number is, respectively, 10^{-7}, 10^{-6}, 10^{-5}, 10^{-4}, 10^{-3}, and 10^{-2}. In Panel (b), the Richardson number is 0.01, 0.05, 0.1 and 0.15 for curve 1 to curve 4, respectively.

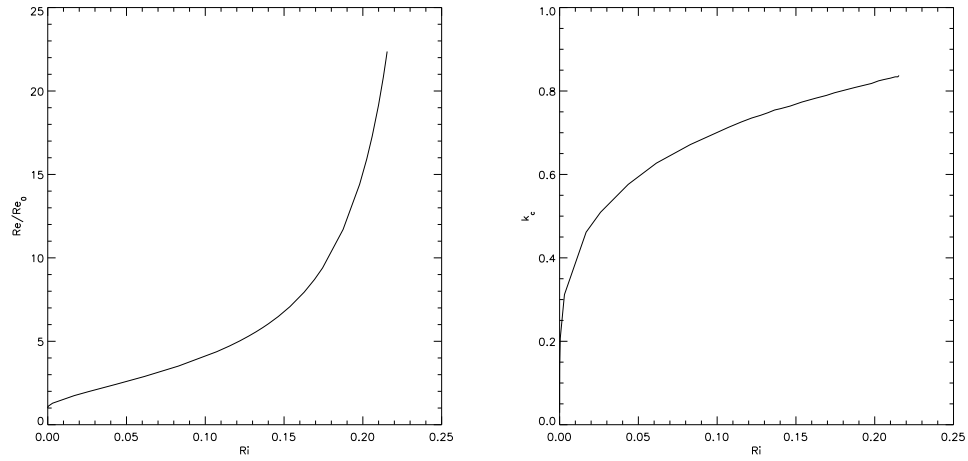

(a) (b)

Figure 2: Critical Reynolds number (a) and critical wave number (b) as functions of Richardson number for Pr = 10 for the periodic case.

2.3 Linear analysis on the stratified Kolmogorov flow: Floquet calculation

We now show results from the Floquet calculation for the stratified Kolmogorov shear flow. We perturb the system with perturbation of the form: $e^{iqz+ikx}\psi(z,t)$, where $0 \leq q \leq 0.5$ is the Floquet multiplier (Bloch number) and k is the horizontal wave number. With the definition of ∇'^2 in equation 9,

$$\nabla'^2\psi \equiv -(k^2+q^2)\psi + 2iq\partial_z\psi + \partial_z^2\psi, \tag{9}$$

equations 6 and 7 then take the following form:

$$\partial_t\nabla'^2\psi - \sin z\; ik(\nabla'^2\psi + \psi) = \frac{1}{\mathrm{Re}}\nabla'^4\psi - ik\mathrm{Ri}\theta, \tag{10}$$

$$\partial_t\theta - ik(\sin z\;\theta + \psi) = \frac{1}{\mathrm{Pe}}\nabla'^2\theta. \tag{11}$$

Solving equations 10 and 11 numerically with periodic boundary conditions, we obtain the parametric marginal curves for various values of q. Figure 3 shows the critical Reynolds number as a function of q for the non-stratified (Ri = 0) case. We first note that $\mathrm{Re}_c(q) \geq \mathrm{Re}_c(q=0)$, and at around $q = 0.35$ the minimum moves from one branch to the other, thus a cuspy transition at $q = 0.35$. From figure 3 we also note that the most unstable mode has the same periodicity as the background shear flow. Therefore, we do not need to perform the same Floquet calculation for the stratified case. Having shown that perturbations of the same periodicity are the most unstable, we then proceed to uncover the effect of weak stratification on the nonlinear behavior of the flow. By this we in particular mean that we are going to perform amplitude expansion around the $k = 0$ mode for small Ri. From the

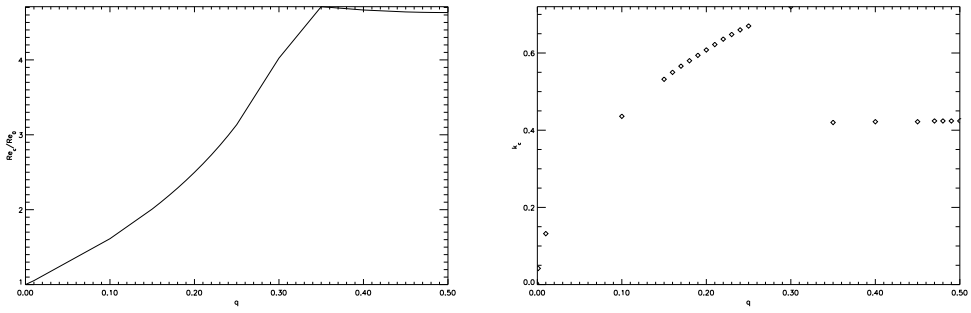

(a) (b)

Figure 3: Critical Reynolds number (a) and critical wave number (b) as functions of the Floquet multiplier q for the non-stratified Kolmogorov shear flow.

linear analysis, we have observed that the critical wave number k_c increase from zero (for no stratification, $\mathrm{Ri} = 0$) to finite value (for strong stratification). As k_c transitions from 0 to finite values, the amplitude equation changes from a Cahn-Hilliard like equation [4] for long wavelength instability to a Ginzburg-Landau equation for finite wavelength instability. In our weakly nonlinear analysis, we focus on the weak stratification limit where the system still inherits the instability to long wavelength perturbation. To have buoyancy (θ) appear at the desired order in the amplitude equation, we rescale θ and put Ri to small numbers such that $\mathrm{Ri} \equiv \epsilon^6 F_6$ and $b \equiv \mathrm{Ri}\theta/\epsilon^5 = \epsilon F_6 \theta$. Equations 4 and 5, in the new scaling, take the following form:

$$\epsilon^4 \partial_\tau \nabla^2 \psi - \epsilon J_\xi(\psi, \nabla^2 \psi) - \epsilon \sin z (\nabla^2 \psi + \psi)_\xi = \frac{1}{\mathrm{Re}}(1-\epsilon^2)\nabla^4 \psi - \epsilon^6 b_\xi, \tag{12}$$

$$\epsilon^4 \partial_\tau b - \epsilon J_\xi(\psi, b) - \epsilon^2 F_6 \psi_\xi - \epsilon \sin z b_\xi = \frac{1}{\mathrm{Pe}} \nabla^2 b, \tag{13}$$

where J_ξ is the usual Jacobian with respect to ξ and z.

3 Weakly nonlinear analysis: $\mathrm{Pe} \sim \mathcal{O}(1)$

In this section we first construct the amplitude equations for the stratified shear flow with $\mathrm{Pe} \sim \mathcal{O}(1)$. We remark here that we are mostly interested in two ranges of Pe: $\mathrm{Pe} \sim \mathcal{O}(1)$ and $\mathrm{Pe} \gg 1$. The range $\mathrm{Pe} \ll 1$ is where molecular diffusivity dominates the dynamics, and to first few orders in the expansion, there appears to be no coupling between the temperature and the flow, and thus is of no interests in our analysis. In real physical systems (salty water, for example), the Pelect number for a small Reynold number of $\sqrt{2}$ is already on the order of a thousand, and thus cases where $\mathrm{Pe} \gg 1$ are of more physical relevance. In subsection 3.3 we present numerical solutions to the amplitude equations for the $\mathrm{Pe} \sim \mathcal{O}(1)$ case. In the following section, we derive the amplitude equation for the nondiffusive case ($\mathrm{Pe} \gg 1$).

3.1 Construction of the amplitude equations: $\mathrm{Pe} \sim \mathcal{O}(1)$

Adopting the scaling discussed in section 2.2, and expanding ψ and θ as follows

$$\psi = \psi_0 + \epsilon\psi_1 + \epsilon^2\psi_2 + \epsilon^3\psi_3 + \cdots, \tag{14}$$
$$\theta = \theta_0 + \epsilon\theta_1 + \epsilon^2\theta_2 + \epsilon^3\theta_3 + \cdots, \tag{15}$$

we substitute the above expansions into equations 12 and 13. Collecting terms order by order, (ψ_i, θ_i) that satisfy the periodic boundary conditions (for the "fast variable" z) are obtained, and the solvability condition at each order gives rise to relationships between ψ_i and θ_i. At the zeroth order $\mathcal{O}(\epsilon^0)$, the equations are:

$$\psi_{0zzzz} = 0, \qquad \frac{1}{\mathrm{Pe}} b_{0zz} = 0, \tag{16}$$

and the periodic solutions are

$$\psi_0 = A(\xi, \tau), \qquad b_0 = B(\xi, \tau). \tag{17}$$

At the first order $\mathcal{O}(\epsilon^1)$, we obtain the following equations

$$\frac{1}{\mathrm{Re}} \psi_{1zzzz} = -A_\xi \sin z, \tag{18}$$
$$\psi_{0z} B_\xi - \psi_{0\xi} B_z = \frac{1}{\mathrm{Pe}} b_{1zz}, \tag{19}$$

and the periodic solutions

$$\psi_1 = -\mathrm{Re} A_\xi \sin z + A_1(\xi, \tau), \qquad b_1 = \mathrm{Pe} B_\xi \sin z + B_1(\xi, \tau). \tag{20}$$

At the second order $\mathcal{O}(\epsilon^2)$, the equations are as follows:

$$\frac{1}{\mathrm{Re}} \psi_{2zzzz} = -A_{1\xi} \sin z - \mathrm{Re} A_\xi^2 \cos z, \tag{21}$$

$$\frac{1}{\mathrm{Pe}} b_{2zz} = -B_{1\xi} \sin z - (\mathrm{Re} + \mathrm{Pe}) A_\xi B_\xi \cos z - (\frac{\mathrm{Pe}}{2} + \frac{1}{\mathrm{Pe}}) B_{\xi\xi} - F_6 A_\xi + \frac{\mathrm{Pe}}{2} B_{\xi\xi} \cos 2z. \tag{22}$$

At this order $\mathcal{O}(\epsilon^2)$, the solvability condition for ψ_2 gives rise to the critical Reynolds number $\mathrm{Re} = \mathrm{R}_0 \equiv \sqrt{2}$. The solvability condition for θ_2 gives us the following relationship between $B(\equiv \theta_0)$ and $A(\equiv \psi_0)$:

$$(\frac{\mathrm{Pe}}{2} + \frac{1}{\mathrm{Pe}}) B_{\xi\xi} + F_6 A_\xi = 0. \tag{23}$$

The solutions at this order are:

$$\psi_2 = -\mathrm{R}_0 A_{1\xi} \sin z - {\mathrm{R}_0}^2 A_\xi^2 \cos z + A_2(\xi, \tau), \tag{24}$$
$$b_2 = \mathrm{Pe} B_{1\xi} \sin z + \mathrm{Pe}(\mathrm{R}_0 + \mathrm{Pe}) A_\xi B_\xi \cos z - \frac{\mathrm{Pe}^2}{8} \cos 2z B_{\xi\xi}. \tag{25}$$

Going on to the 3rd order in ϵ, we have the following equations for ψ_3:

$$\frac{1}{\mathrm{R}_0}\psi_{3zzzz} = [{\mathrm{R}_0}^2 A_\xi^3 - 3A_{\xi\xi\xi} - A_\xi - A_\xi^2]\sin z - 2{\mathrm{R}_0}^2 A_{1\xi}A_\xi \cos z, \tag{26}$$

and the solution ψ_3 is easily obtained as follows:

$$\psi_3 = \mathrm{R}_0[{\mathrm{R}_0}^2 A_\xi^3 - 3A_{\xi\xi\xi} - A_\xi - A_{2\xi}]\sin z - 2{\mathrm{R}_0}^3 A_{1\xi}A_\xi \cos z + A_3(\xi,\tau). \tag{27}$$

The solvability condition at this order gives us the amplitude equation:

$$(A_{\xi\xi})_\tau + \frac{3\mathrm{R}_0}{2}A_{\xi\xi\xi\xi\xi\xi} + \{[\mathrm{R}_0 - \frac{{\mathrm{R}_0}^3}{3}A_\xi^2]A_\xi\}_{\xi\xi\xi} - \frac{F_6}{\mathrm{Pe}/2 + 1/\mathrm{Pe}}A = 0. \tag{28}$$

Following Sivashinsky, if we write $\partial_z = \partial_z + \epsilon^3\partial_\eta$, we obtain identical solutions till the second order and obtain the following amplitude equation at third order:

$$\begin{aligned}(A_{\xi\xi})_\tau &= -\frac{3\mathrm{R}_0}{2}A_{\xi\xi\xi\xi\xi\xi} - \{[\mathrm{R}_0 - \frac{{\mathrm{R}_0}^3}{3}A_\xi^2]A_\xi\}_{\xi\xi\xi} \\ &\quad -A_\eta A_{\xi\xi\xi} + A_\xi A_{\xi\xi\eta} + \frac{{\mathrm{R}_0}^2}{2}(A_\xi)^2_{\xi\eta} + \frac{F_6}{\mathrm{Pe}/2 + 1/\mathrm{Pe}}A.\end{aligned} \tag{29}$$

We note that the buoyancy amplitude B is completely slaved to the stream function amplitude A as the effect of the stabilizing temperature gradient is put to higher order (ϵ^6). Writing $\rho = \xi + c\eta$, we can turn equation 29 into a uni-directional amplitude equation [1] in terms of ρ and τ as follows:

$$(A_{\rho\rho})_\tau = -\frac{3\mathrm{R}_0}{2}A_{\rho\rho\rho\rho\rho\rho} - \{[\mathrm{R}_0 - \frac{{\mathrm{R}_0}^3}{3}A_\rho^2]A_\rho\}_{\rho\rho\rho} + \frac{c{\mathrm{R}_0}^2}{2}(A_\rho)^2_{\rho\rho} + \frac{F_6}{\mathrm{Pe}/2 + 1/\mathrm{Pe}}A, \tag{30}$$

where c is the aspect ratio of the characteristics of the uni-directional flow.

3.2 Lyapunov functional

In this subsection we derive a Lyapunov functional for the 1D amplitude equation (equation 28). Following [7], we try to find an energetic functional of amplitude A such that the evolution of the amplitude can be described by the functional. To be more specific, we seek a Lyapunov functional $V[A]$ such that

$$\partial_\tau A = -\frac{\delta V[A]}{\delta A}, \qquad \partial_\tau V = -\int (A(\xi,\tau)_\tau)^2 d\xi, \tag{31}$$

which then implies that the system cannot sustain oscillatory motion and has to settle down to a stationary equilibrium. For the 1D amplitude equation for the weakly stratified case, it is straightforward to find a functional for the amplitude equation 28 if we rewrite it as follows:

$$(A_{\xi\xi})_\tau = -\partial_\xi^2\frac{\delta F}{\delta A} + \frac{F_6}{\mathrm{Pe}/2 + 1/\mathrm{Pe}}A, \tag{32}$$

where

$$F[A] \equiv -\frac{1}{4}\int 4A_\xi^2 - A_\xi^4 - 2A_{\xi\xi}^2 d\xi. \tag{33}$$

Putting $C_{\xi\xi} \equiv A$, we write down the evolution equation for F as:

$$\frac{dF}{d\tau} = -\int A_\tau^2 d\xi - \frac{F_6}{\mathrm{Pe}/2 + 1/\mathrm{Pe}}\partial_\tau \int \frac{C_\xi^2}{2} d\xi. \tag{34}$$

This indicates that the new functional $G \equiv F + \frac{F_6 \mathrm{Pe} C_\xi^2}{\mathrm{Pe}^2+2}$ is decaying in time and there is a stationary solution for arbitrary initial conditions. In the absence of the stabilizing stratification, random perturbation of small scales will reach a stationary solution with minimum number of nodes within the domain, i.e., the scale of the stationary solution is the size of the domain. This is the essence of inverse cascade: the evolution of the amplitude is such that the spatial scale increases until it reaches the scale comparable to the size of the computation domain. In the nonstratified case, since the functional is expressed in the gradient of A, an the fact that A is periodic in ξ, we conclude that the stationary solution $A(\xi)$ should have only one bump inside the domain. However, this inverse cascade is arrested by the presence of stabilizing stratification, as the additional term C_ξ included in the functional prevents the inverse cascade process. This will be demonstrated in the following subsection.

3.3 Numerical solution

In this section we present numerical results from solving the amplitude equations using a pseudo-spectral code. First we show results for the 1D version of the amplitude equation (equation 28). Figure 4 demonstrates the stabilizing effect of the temperature: the amplitude decreases and the structure tends to be of smaller scale as we increase the strength of stratification. As shown in the previous subsection, we can find a Lyapunov functional for this equation in terms of the gradient of the amplitude, therefore, we display the temporal evolution of the amplitude gradient (figure 5). Figures 5 show the time-space plots for the gradients of the amplitudes without any stratification in (a) and with an $F_6 = 0.1$ in (b). We note that the inverse cascade manifested in panel (a) is arrested by the presence of stabilizing stratification in panel (b), in agreement with the conclusion we draw from the Lyapunov functional. The numerical solutions to the uni-directional amplitude equation (equation 30) are displayed in figures 6, where the time evolution is for the amplitudes, not the amplitude gradients. In panel (a) of figures 6, where there is no stratification, we see the chaotic behavior of the flow due to the extra nonlinear term. Yet in panel (b) where $F_6 = 0.1$, we see the stratification diminishes the chaotic behavior and reduces the flow to spatially periodic.
In figures 7 we show the solutions $(\Psi_0 + A(\xi, \eta, \tau))$ to the 2-D amplitude equation, where the computation domain has been scaled by an aspect ratio $c = 20$ as suggested in [3]. The only difference between these two snapshots of the stream functions is the stratification strength. We note that the effect of stratification is manifested not only by the change in the amplitude of the flow but also the flow patterns: the stronger the stratification, the smaller the scales are for the flow patterns.

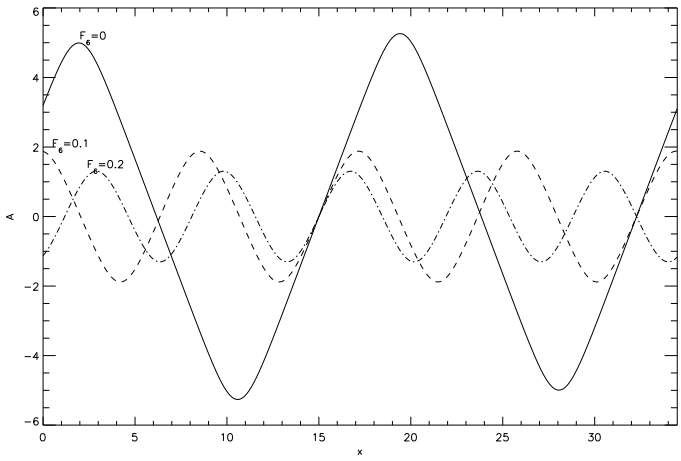

Figure 4: Numerical solutions at $t = 300$ for various strengths of weak stratification.

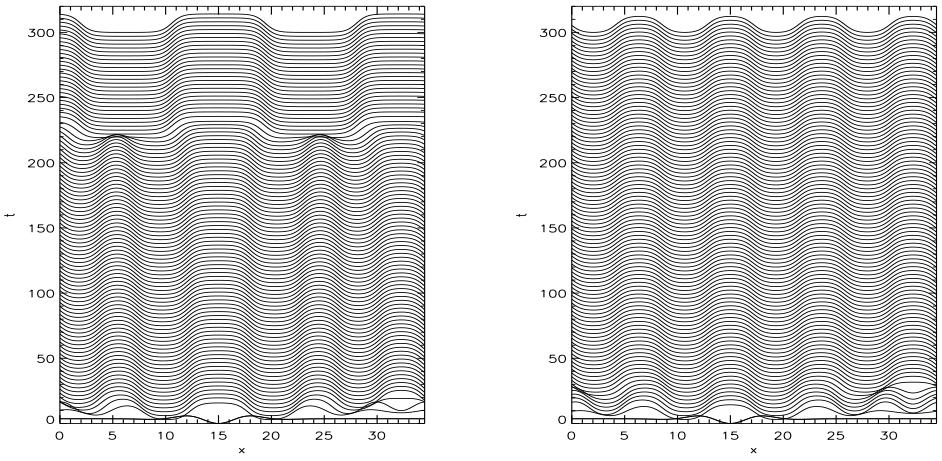

(a) (b)

Figure 5: Time-space plots of the amplitude gradient with $F_6 = 0$ (a) and $F_6 = 0.1$ (b).

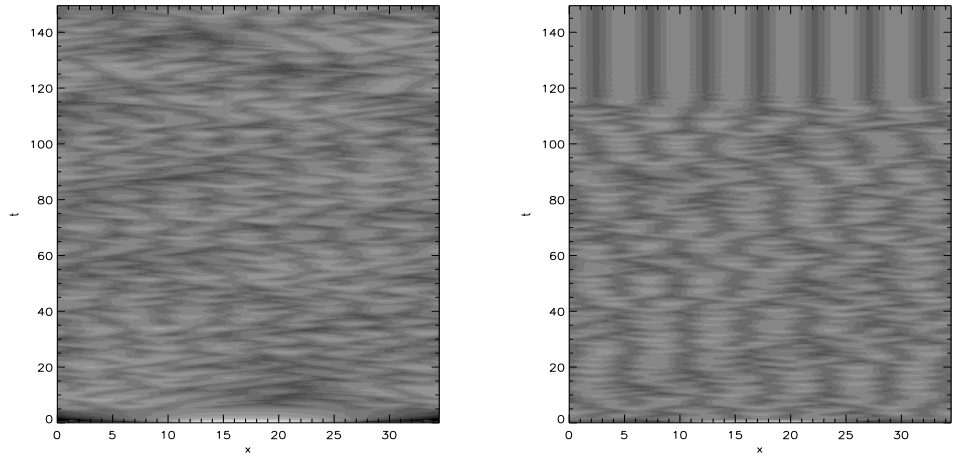

(a) (b)

Figure 6: Time-space plots of the amplitude for the uni-directional flow with $F_6 = 0$ (a) and $F_6 = 0.1$ (b).

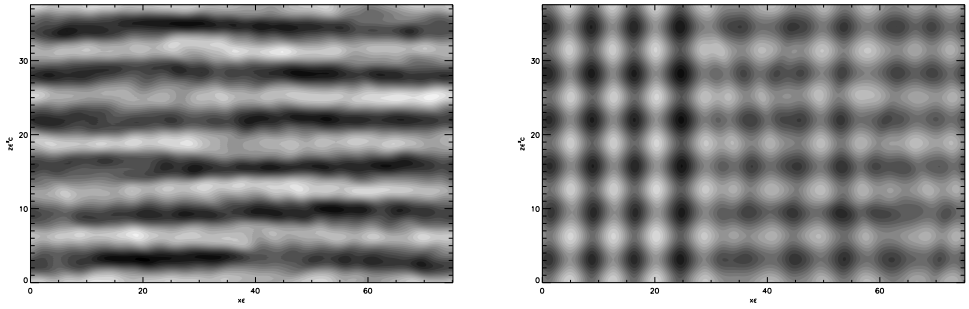

(a) (b)

Figure 7: Stream function (zeroth order) from the 2D amplitude equation for (a) $F_6 = 0.01$ at $t = 15$ and (b) $F_6 = 0.1$.

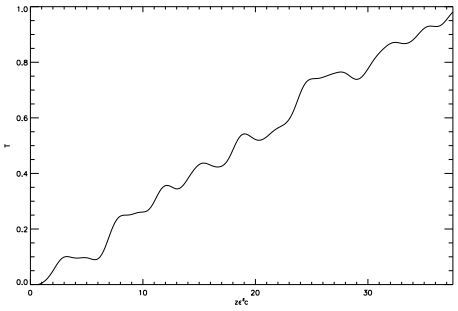

Figure 8: Snapshot of the horizontal average of the total temperature profile for $F_6 = 0.01$.

In figures 8 and 9 we show the horizontal average of the temperature to demonstrate the potential of layer formation in the temperature. Figure 8 is a snapshot of the horizontal average temperature: $\overline{T_0(z) + B(\xi, \eta, t)}$. We note that in Panel (a) of figure 9, layers disappear and re-appear randomly, while in Panel (b) layer structures eventually disappear due to the stabilizing stratification which diminishes the flow.

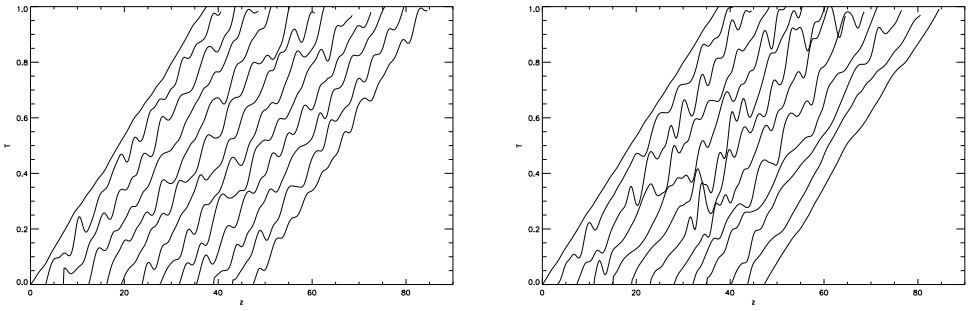

(a) (b)

Figure 9: Horizontal average of the total temperature profile at various times for (a) $F_6 = 0.01$ and (b) $F_6 = 0.1$.

4 Internal Boundary Layer for large Peclet numbers: $\mathrm{Pe} \to \infty$

In this section we focus on the instability of the stratified shear flow in the large Peclet number limit. Figure 10 displays characteristics of the eigenfunctions of the stratified shear flow: the stream function disturbance reaches local minima while the temperature peaks at the inflection point of the background shear flow.

The above structure reminds one of the no-slip, no-flux boundary layer: velocities vanish at the walls and so does the density flux. This is similar to what we observe from the eigen function (for the unbounded case) except that there is a constant background vertical velocity if the horizontal wave number k is not zero. Figures 11 show the internal boundary layer

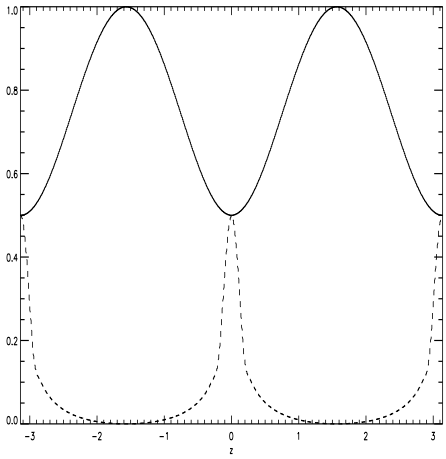

Figure 10: Eigenfunctions for stratified shear flow. The Prandtl number $\mathrm{Pr} = 10^4$ and $\sin z$ is the background shear flow. The solid line is for the stream function disturbance ψ and the dashed line is the temperature disturbance θ.

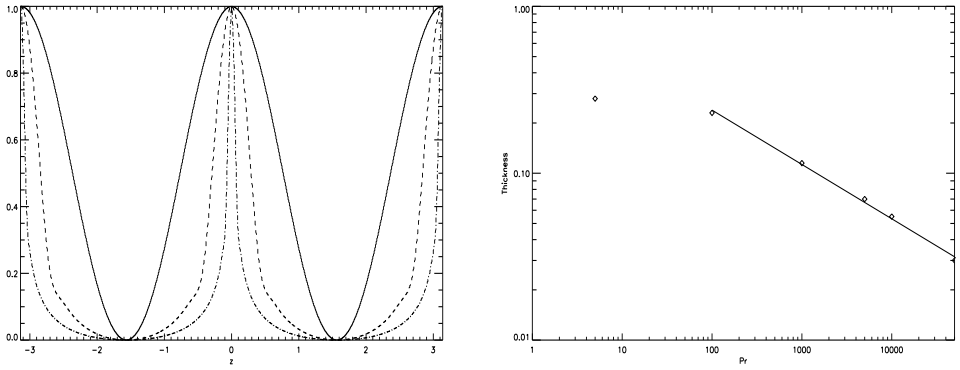

(a) (b)

Figure 11: (a) Internal boundary layer structure as the Prandtl number Pr increases. The Prandtl numbers for the solid, dashed, and dash-dotted lines are, respectively, 10, 10^3, and 10^5. (b) The boundary layer thickness as a function of Pr (note that since the Reynolds number is fixed, the Peclet number is proportional to the Prandtl number). The solid line is the best fit for the last five points, which indicate that the thickness scales to $\mathrm{Pe}^{-0.326}$. The Richardson number Ri is fixed at 0.01 and the Reynolds number is $\mathrm{Re} = 1.92$.

structure as we vary the Prandtl number. We observe the decrease of the internal boundary layer thickness as we decrease the molecular diffusivity. By balancing the advective term (associated with the background shear flow) and the diffusive term, we obtain a naive scaling of the boundary layer thickness (l) with the Peclet number Pe:

$$l \sim \mathrm{Pe}^{-1/3}, \tag{35}$$

which is in fair agreement with the empirical fit obtained from the numerical solutions to the linearized equations. Also in this limit of large (or infinite) Peclet number, the scaling and expansion used in previous section to derive the amplitude equations no longer work inside the "internal boundary layer" as terms of different orders are mixed up. Thus we need to find a new scaling inside the internal boundary layer and perform asymptotic matching across the internal boundary layer. We first perform asymptotic matching for infinite Peclet number cases, and then relax the infinite Peclet number limit to large Peclet number limit (ϵ^{10}) and derive the dispersion relations and general linear solutions in subsection 4.2.

4.1 Scaling and asymptotic matching for the internal boundary layer

We first focus on the linearized version of equation 13 and put right hand side to zero:

$$\epsilon^2 \partial_\tau \theta + \sin z \theta_\xi - \psi_\xi = 0. \tag{36}$$

The zeroth order solution is (A is the amplitude for the stream function disturbance as defined in 3.1)

$$\theta_0 = \frac{\psi_0}{\sin z} = \frac{A}{\sin z}. \tag{37}$$

The solutions for the first and the second order are:

$$\theta_1 = \frac{\psi_1}{\sin z}, \qquad \theta_2 = \frac{\psi_2}{\sin z}. \tag{38}$$

The third order solution takes the following form:

$$\theta_{3\xi} \quad = \quad \frac{\psi_{3\xi}}{\sin z} - \frac{\psi_{0\tau}}{\sin^2 z}. \tag{39}$$

As the background shear flow goes to zero at $z = 0$, the "outer" solutions shown above are no longer regular. We therefore need to find different scaling around $z = 0$ to avoid this embarrassment by matching the above "outer" solution to the "inner" solution, to be derived in the following with the new scaling. The new scaling we adopt is as follows: around $z = 0$ we scale $z = \epsilon^3 Z$ and $\theta = \epsilon^{-3}\Theta$. The rescaled, linearized equation takes the following form:

$$\partial_\tau \Theta + Z\Theta_\xi - \psi_\xi = 0, \tag{40}$$

where we have replaced $\sin z$ with $\epsilon^3 Z$. To perform the matching between inner and outer solutions, we first write the inner solution Θ as

$$\Theta = \frac{A}{Z} + \frac{B}{Z^2} + \cdots \tag{41}$$

where A is the stream function amplitude and B is to be determined by matching the inner solution to the outer solution. We then express the outer solution (full solution to the third order) in terms of the rescaled coordinate Z inside the internal boundary layer:

$$\begin{aligned}\theta &= \frac{A}{\sin z} + \epsilon\frac{\mathrm{R}_0 A_\xi \sin z}{\sin z} + \epsilon^2\frac{\mathrm{R}_0 A_{1\xi}\sin z + {\mathrm{R}_0}^2 A_\xi^2 \cos z + A_2}{\sin z} + \epsilon^3(\frac{\psi_3}{\sin z} - \frac{C}{\sin^2 z}), \quad (42)\\ &= \frac{A}{\epsilon^3 Z} + \epsilon \mathrm{R}_0 A_\xi + \epsilon^2[\mathrm{R}_0 A_{1\xi} + \frac{{\mathrm{R}_0}^2 A_\xi^2(1-\epsilon^6) + A_2}{\epsilon^3 Z}] + \epsilon^3(\frac{\psi_3}{\epsilon^3 Z} - \frac{C}{\epsilon^6 Z^2}), \quad (43)\end{aligned}$$

where $C_\xi = A_\tau$. The leading order term in equation 43 (order ϵ^{-3})

$$\theta \sim \frac{1}{\epsilon^3}(\frac{A}{Z} - \frac{C}{Z^2}) + \mathcal{O}(\epsilon^{-1}) \quad (44)$$

gives us the undetermined B as follows:

$$B_\xi + A_\tau = 0. \quad (45)$$

Having shown how the asymptotic matching works in the internal boundary layer, we press on to find the consistent scaling for the Peclet number. Adopting the same scaling for the inner solution above, we have to put Pe to order ϵ^{-10} to have the diffusive term appeared at the first order in the equation for Θ inside the internal boundary layer:

$$\partial_\tau \Theta + (Z\Theta - \psi)_\xi = \frac{1}{P_{10}}\Theta_{ZZ}. \quad (46)$$

We first note that the boundary conditions for the above linear equation have to be found by matching the inner solution to the outer solution. Secondly, we note that the zeroth order term Θ_0 has non trivial Z and ξ dependence, in contrary to what we have found for $\mathrm{Pe} \sim \mathcal{O}(1)$ cases.

4.2 Amplitude equation and the dispersion relation

The previous analysis shows that, in the limit of large Peclet number, Θ depends on Z as well as ξ and τ . With this in mind, we proceed from equations 12 and 13 to write down the amplitude equation for the internal boundary layer. First we note that as the strength of stratification is put to ϵ^6, the solutions for the stream function obtained in section 3.1 are still valid in the internal boundary layer. We then only need to concentrate on the heat equation for θ:

$$\partial_t \theta - J(\psi, \theta) + \sin z \partial_x \theta - \partial_x \psi = \frac{1}{\mathrm{Pe}}\nabla^2 \theta \quad (47)$$

Adopting the scaling $\partial_t = \epsilon^4 \partial_\tau$, $\partial_x = \epsilon \partial_\xi$, $\partial_z = \epsilon^{-3}\partial_Z$ and $\theta = \epsilon^{-3}\Theta$ the above equation takes the following form:

$$\epsilon\partial_\tau \Theta - \epsilon^{-5} J(\psi, \Theta) + \epsilon(Z\Theta_\xi - \psi_\xi) = \frac{\epsilon}{P_{10}}\Theta_{ZZ}. \quad (48)$$

Rescaling $\Theta' = \epsilon^6\Theta$, $\psi' = \epsilon^6\psi$ and dropping the primes, we arrive at the following equation for the temperature disturbance inside the internal boundary layer:

$$\partial_\tau\Theta - J(\psi,\Theta) + Z\Theta_\xi - \psi_\xi = \frac{1}{P_{10}}\Theta_{ZZ}. \tag{49}$$

The stream function amplitude A satisfies the same equation 28 except that inside the internal boundary layer, the average of Θ_x over Z is not simply Θ_x as Θ depends on Z as well. Also, we have to rescale A accordingly inside the internal boundary layer, so all the nonlinear terms in equation 28 drop out and we obtain the following equation:

$$\partial_\tau A_{\xi\xi} = -\mathrm{R}_0(\frac{3}{2}A_{\xi\xi} + A)_{\xi\xi\xi\xi} - F_6\int_{\text{“}-\infty\text{”}}^{\text{“}\infty\text{”}}\Theta_\xi dZ, \tag{50}$$

where the integral range (“$-\infty$”, “∞”) is referred to the scaled internal boundary layer. To zeroth order in ϵ, we obtain the following equation:

$$\partial_\tau\Theta - A_\xi\Theta_Z + Z\Theta_\xi - A_\xi = \frac{1}{P_{10}}\Theta_{ZZ}, \tag{51}$$

where $A = A(\xi,\tau)$ is the amplitude for the stream function. Equations 50 and 51 are the amplitude equations for the internal boundary layer. The linear equations for the internal boundary layer are

$$\partial_\tau A_{\xi\xi} = -\mathrm{R}_0(\frac{3}{2}A_{\xi\xi} + A)_{\xi\xi\xi\xi} - F_6\int_{-\infty}^{\infty}\Theta_\xi dZ, \tag{52}$$

$$\partial_\tau\Theta = -Z\Theta_\xi + A_\xi + \frac{1}{P_{10}}\Theta_{ZZ}. \tag{53}$$

We first derive the dispersion relation for the infinite Peclet number case. Replacing ∂_ξ with ik and ∂_τ with s, we obtain the following equations:

$$-k^2[s + \frac{3\mathrm{R}_0}{2}k^4 - \mathrm{R}_0k^2]A = -F_6\int_{-\infty}^{\infty}ik\Theta dZ, \tag{54}$$

$$(s + iZk)\Theta = ikA. \tag{55}$$

Substituting equation 55 into 54, we obtain the dispersion relation for the infinite Peclet number case:

$$s = -\frac{F_6}{|k|}sgn(s)\pi - \frac{3\mathrm{R}_0}{2}k^4 + \mathrm{R}_0k^2. \tag{56}$$

In the case of finite, large Peclet numbers, we expand Θ in both e^{ikx} and e^{iqz} and obtain the following equations

$$-(s + kq^2)\widetilde{\Theta} + \widetilde{\Theta}_q = -2\pi i\widetilde{A}\delta(q), \tag{57}$$

where $\widetilde{\Theta}$ and $\widetilde{A}$ are Fourier components in the $k-q$ spectral space. The solution to equation 57 is

$$\widetilde{\Theta} = e^{(sq+kq^3/3)/k}\int_q^\infty 2\pi i\widetilde{A}\delta(q')e^{-(sq'+kq'^3/3)/k}dq' \tag{58}$$

$$= e^{(sq+kq^3/3)/k}2\pi i\widetilde{A}H(-q), \tag{59}$$

where H is the Heaviside function. Substituting the above normal mode solution for $\widetilde{\Theta}$ into 52, we get the dispersion relation for the large, finite Peclet number case:

$$s = -\frac{F_6}{|k|}\pi - \frac{3\mathrm{R}_0}{2}k^4 + \mathrm{R}_0 k^2. \tag{60}$$

We note the difference between equation 56 and 60 is the existence of $sgn(s)$, and we display the two dispersion relations in figure 12.

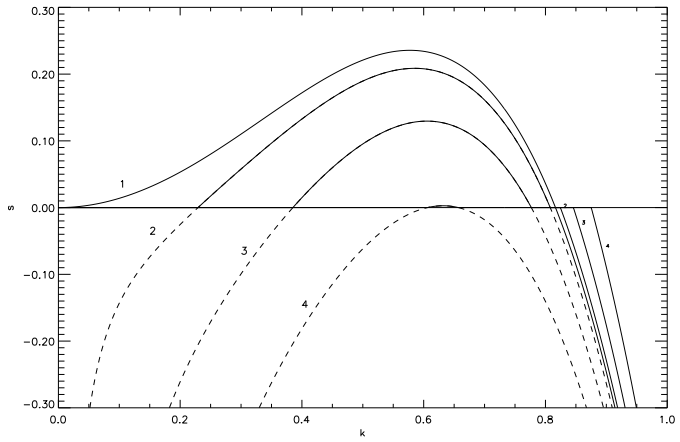

Figure 12: Dispersion relation for the internal boundary layer ($\mathrm{R}_0 = \sqrt{2}$). Curves are labeled by the scaled Richardson number F_6: From curve 1 to curve 4, F_6 are, respectively, 0, 0.005, 0.02, 0.045. The solid lines are for the infinite Peclet number cases, and the dotted lines are for large Peclet number cases.

We also note that for any given Reynolds number, the value of F_6 such that the maximum growth rate s is zero is proportional to the Reynolds number and the ratio is 0.0322. We are now ready to find the general solution to Θ for large Peclet number cases. We rewrite equation 53 as follows:

$$\kappa\Theta_{ZZ} - (s + ikZ)\Theta = ikA, \tag{61}$$

where $\kappa = 1/P_{10}$. Dividing the above equation by ikA and denote $f \equiv \Theta/ikA$, we obtain the following equation which allows us to find a closed-form solution:

$$\kappa f_{ZZ} - ik(Z - is/k)f = 1. \tag{62}$$

The solution is the Yi function:

$$\Theta = \frac{i\pi A}{k\kappa}\mathrm{Yi}[k(Z - is/k)]. \tag{63}$$

5 Inviscid limit of the stratified, Kolmogorov shear flow

In this section we conclude the report by presenting a brief study on the inviscid limit of the stratified Kolmogorov shear flow. A general review on linear analysis of the inviscid shear flow

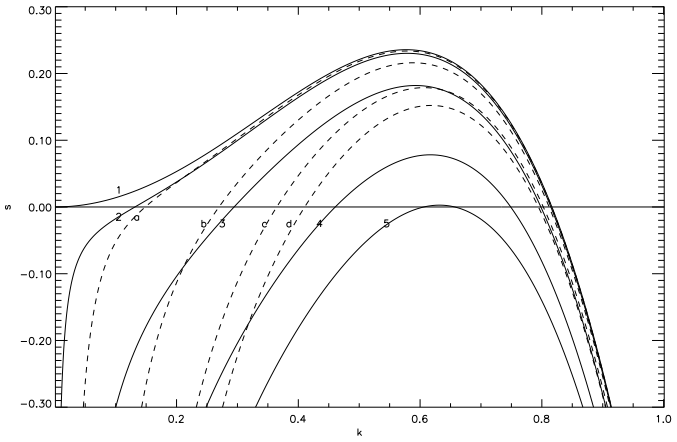

Figure 13: Dispersion relation for the internal boundary layer ($\mathrm{R}_0 = \sqrt{2}$). Dashed lines are for order $\mathcal{O}(1)$ Peclet numbers and solid lines are for large Peclet numers. Curve '1' is for $F_6 = 0$, curves '2' and 'a' are for $F_6 = 0.001$, curves '3' and 'b' are for $F_6 = 0.01$, curves '4' and 'c' are for $F_6 = 0.03$, and curves '5' and 'd' are for $F_6 = 0.045$.

can be found in [8]. Here we provide a way to find neutral states for the unbounded, stratified Kolmogorov shear flow. We have numerically verified the marginal boundary presented in the following analyses, and it would be an interesting direction to provide analytic proofs that this is indeed the case. We should also point out that there may be hope to couple the critical layers (CL) associated with each inflection point in the background shear flow, and hence the interaction between CLs can be investigated.

5.1 Linear analysis: analytical and numerical

The inviscid, nondiffusive system ($1/\mathrm{Pe} = 0$) is described as follows (where the shear flow is a sinusoidal $\sin z$ in a periodic domain):

$$\partial_t \nabla^2 \psi - J(\psi, \nabla^2 \psi) + \sin z \partial_x (\nabla^2 \psi + \psi) = -F \partial_x \theta, \tag{64}$$

$$\partial_t \theta - J(\psi, \theta) + \sin z \partial_x \theta - \partial_x \psi = 0. \tag{65}$$

The linearized equations can be put into the following equation with the diffusivity being zero:

$$(\sin z - c)(D^2 - k^2)\psi + \sin z \psi = -\frac{F\psi}{\sin z - c}, \tag{66}$$

where $D \equiv \partial_z$ and c is growth rate divided by the wave number. In this notation, the imaginary part of c indicates instability: positive imaginary part means growing mode and negative imaginary part means decaying mode. We reorganize the above equation into a more familiar form usually found in the past literature:

$$\psi'' - k^2 \psi + \frac{\sin z \psi}{\sin z - c} = -\frac{F\psi}{(\sin z - c)^2}. \tag{67}$$

First we put $c = 0$, though in general only the imaginary part is required to be zero on the neutral curve. Equation 67 now takes the following form:

$$D^2\psi + (1 - k^2 + \frac{F}{\sin^2 z})\psi = 0. \tag{68}$$

The above equation can be solved as follows: first we put the left hand side of equation 68 as the product of two differential operators as defined as follows:

$$(D^2 + 1 - k^2 + \frac{F}{\sin^2 z})\psi = \mathcal{L}\mathcal{L}^\dagger\psi = 0, \tag{69}$$

where $\mathcal{L}$ and $\mathcal{L}^\dagger$ are defined as

$$\mathcal{L} \equiv D + \frac{a}{\cot z}, \qquad \mathcal{L}^\dagger \equiv D - \frac{a}{\cot z}, \tag{70}$$

and a is to be determined (in terms of k and F). We note that $\mathcal{L}\mathcal{L}^\dagger = D^2 - (f' + f)$ where $f = \cot z$, and relationships between a, k, and F are obtained as follows:

$$a = 1 - k^2, \qquad F = a - a^2 = \sqrt{1 - k^2} - (1 - k^2). \tag{71}$$

The first solution ψ_1 is obtained by demanding $\mathcal{L}\psi_1 = 0$ and takes the following form:

$$\psi_1 = (\sin z)^{\sqrt{1-k^2}}, \;\; z \geq 0. \tag{72}$$

The second solution ψ_2 satisfies the following equation

$$\mathcal{L}^\dagger\psi_2 = (\sin z)^{-\sqrt{1-k^2}}, \tag{73}$$

and is obtained as follows:

$$\psi_2 = (\sin z)^{\sqrt{1-k^2}} \int^z (\sin z')^{-2\sqrt{1-k^2}} dz'. \tag{74}$$

For some value of k, the second solution is not periodic in z and therefore is not of particular interest. F, as a function of k, is shown in figure 14. First we note that the maximum value of F is $1/4$ when $k = \sqrt{3/4}$. We also note that k goes from 0 to 1 as we are only interested in positive F.

6 Conclusion

We have investigated the effect of stabilizing stratification on the Kolmogorov shear flow in the weak limit where the long wavelength instability inherits from the non-stratified shear flow. Concentrating on cases where $\mathrm{Pe} \sim \mathcal{O}(1)$, we first derived amplitude equations for the weakly stratified Kolmogorov shear flow and demonstrated the stabilizing effects by numerically solving the amplitude equations. For the 1-D amplitude equation, the stabilizing gradient arrests the inverse cascade and weaken the flow. For the uni-directional amplitude equation,

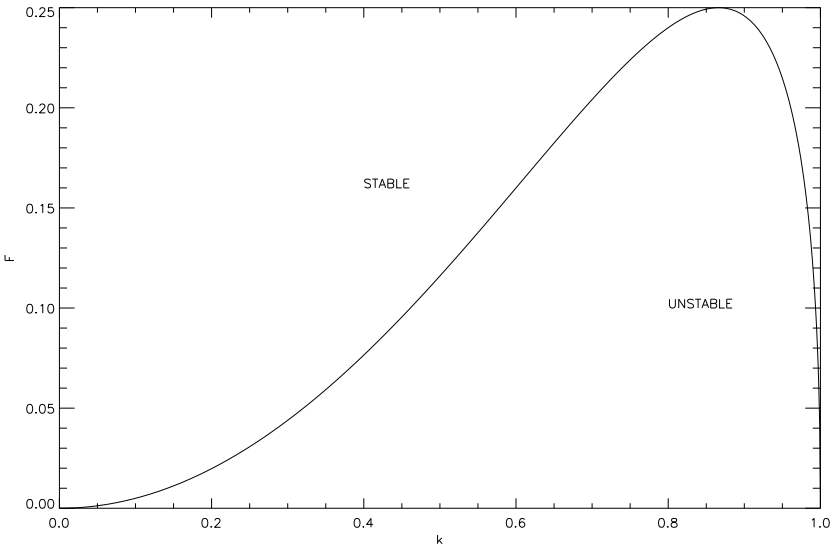

Figure 14: Stability boundary for the inviscid, non-diffusive limit.

the gradient not only lessens the flow, but also diminishes the chaotic behavior of the unidirectional solution. The same phenomena have been observed for the large aspect ratio 2-d solutions to the full amplitude equation. For the nondiffusive limit (Pe $\sim \epsilon^{-10}$), the dynamics are dominated by the internal boundary layer. From the linear eigenfunctions, we are able to estimate an empirical scaling of boundary layer thickness with the Peclet number. We choose boundary layer scaling accordingly and derive amplitude equations for the internal boundary layer. Dispersion relations are derived and utilized for some preliminary analysis. The linear stability of the stratified, inviscid Kolmogorov shear flow has been investigated as a preliminary step to the weakly nonlinear analysis which is now under investigation.

7 Acknowledgments

The project literally started to take form in the summer of 1998, during my first visit to GFD. Serious development of this project started only at the beginning of this summer under guidance from two key collaborators, Bill Young and Neil Balmforth. I would like to acknowledge, with full sincerity and gratitude, the principal lecturer Bill Young for his infinite patience during this collaboration. I would also like to thank the director Neil Balmforth for his insightful guidance all the way through the collaboration, and great advice he so sincerely provided for the whole summer. Thanks also go to Louis Howard and Willem Malkus for inspiring and useful conversations. Finally, I would like to thank all the staff (Claudia, especially) and my fellow fellows for making this summer quite an unforgettable experience.

References

[1] G. Sivashinsky, "Weak turbulence in periodic flows," Physica D **17**, 243 (1985).

[2] Z. S. She, "Metastability and vortex pairing in the kolmogorov flow," Physics Letter A **124**, 161 (1987).

[3] G. Sivashinsky and V. Yakhot, "Negative viscosity effect in large-scale flows," Phys. Fluids **28**, 1040 (1985).

[4] A. Manfroi and W. Young, "Slow evolution of zonal jets on the beta plane," J. Atmos. Sci. **56**, 784 (1999).

[5] W. J. Park, Y.-G. and A. Gnanadeskian, "Turbulent mixing in stratified fluids: layer formation and energetics," J. Fluid Mech. **279**, 279 (1994).

[6] N. Balmforth and W. Young, "Turbulent stratified fluids," J. Fluid Mech. **400**, 500 (1995).

[7] C. Chapman and M. Proctor, "Nonlinear rayleigh-benard convection with poorly conducting boundaries," J. Fluid Mech. **101**, 759 (1980).

[8] P. Drazin and L. Howard, "Hydrodynamic stability of parallel flow of inviscid fluid," Advances in Applied Mechanics **9**, 1 (1996).